### Title

Supramolecular Interactions of Teixobactin Analogues in the Crystal State.




### Journal

The Journal of Organic Chemistry, 89(7)



### Authors

Yang, Hyunjun

Kreutzer, Adam

Nowick, James



### Publication Date

2024-04-05

### DOI

10.1021/acs.joc.3c02617

Peer reviewed

JOC The Journal of Organic Chemistry



pubs.acs.org/joc
Note

# Supramolecular Interactions of Teixobactin Analogues in the Crystal State

Hyunjun Yang, Adam G. Kreutzer, and James S. Nowick*

Cite This: J. Org. Chem. 2024, 89, 5104−5108



**ABSTRACT:** This Note presents the X-ray crystallographic structure of the *N*-methylated teixobactin analogue *N*-Me-D-Gln$_4$,Lys$_{10}$-teixobactin (**1**). Eight peptide molecules comprise the asymmetric unit, with each peptide molecule binding a chloride anion through hydrogen bonding with the amide NH group of residues 7, 8, 10, and 11. The peptide molecules form hydrogen-bonded antiparallel $\beta$-sheet dimers in the crystal lattice, with residues 1−3 comprising the dimerization interface. The dimers further assemble end-to-end in the crystal lattice.

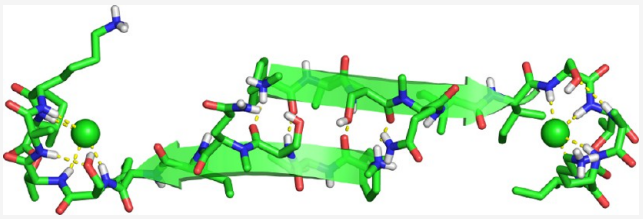

Teixobactin is a peptide antibiotic that exhibits remarkable efficacy against Gram-positive bacteria, including methicillin-resistant *Staphylococcus aureus*, drug-resistant *Streptococcus pneumonia*, and vancomycin-resistant *Enterococci*.[1] Teixobactin's mode of action involves binding to lipid II and related peptidoglycan precursors and disrupting the bacterial cell membrane. Teixobactin is an undecapeptide consisting of an N-terminal linear tail encompassing residues 1−7 and a C-terminal macrocyclic ring spanning residues 8−11 (Figure 1). The linear tail consists of *N*-Me-D-Phe$_1$, Ile$_2$, Ser$_3$, D-Gln$_4$, D-*allo*-Ile$_5$, Ile$_6$, and Ser$_7$, and the macrocyclic ring consists of D-Thr$_8$, Ala$_9$, the cyclic arginine analogue *allo*-End$_{10}$, and Ile$_{11}$. The C-terminus of Ile$_{11}$ and the hydroxy group of D-Thr$_8$ form an ester bond, creating a 13-membered lactone ring.

Supramolecular assembly is central to the mechanism of action of teixobactin.[2,3] Two teixobactin molecules come together to form an antiparallel $\beta$-sheet dimer, which binds the pyrophosphate group of lipid II. The N-terminal tails comprise the dimerization interface and adopt a conformation in which the residues *N*-Me-D-Phe$_1$, Ile$_2$, D-*allo*-Ile$_5$, and Ile$_6$ form a hydrophobic surface that interacts with the bacterial cell membrane. The *allo*-End$_{10}$ residue, although not essential for binding and antibiotic activity, makes additional contacts with the pyrophosphate and MurNAc groups of lipid II that impart enhanced affinity and antibiotic activity. Further supramolecular assembly leads to the clustering of lipid II and the lysis of Gram-positive bacteria.

Our laboratory has pioneered the use of X-ray crystallography to gain insights into the structure and supramolecular interactions of teixobactin. Although teixobactin itself is highly prone to amyloid-like aggregation and cannot be crystallized, our laboratory has found that *N*-methylation at D-Gln$_4$ blocks the aggregation and permits crystallization. The resulting *N*-methylated teixobactin analogues exhibit little or no antibiotic activity. We previously observed that teixobactin analogue 2 undergoes supramolecular assembly to form antiparallel $\beta$-sheet dimers that bind sulfate anions and further form fibril-like assemblies (PDB 6E00).[4] We also observed antiparallel $\beta$-sheet dimers in the X-ray crystallographic structure of teixobactin analogue **3**, and we observed that these dimers bind chloride anions (PDB 6PSL).[5] We further observed chloride anion binding in the X-ray crystallographic structure of truncated teixobactin analogue 4 (CCDC 1523518).[6] In the current study, we report the X-ray crystallographic structure of teixobactin analogue **1** and describe its supramolecular interactions in the crystal state.

The X-ray crystallographic structure of teixobactin analogue **1** reveals eight peptide molecules in the asymmetric unit, with each peptide molecule binding a chloride anion (Figure 2). The eight peptide molecules adopt similar conformations, with a backbone RMSD of 0.58 Å. Each peptide molecule forms an amphiphilic surface in which the side chains of *N*-Me-D-Phe$_1$, Ile$_2$, D-*allo*-Ile$_5$, Ile$_6$, and Ile$_{11}$ and the $\beta$-methyl of D-Thr$_8$ create a hydrophobic surface and the side chains of residues Ser$_3$, *N*-Me-D-Gln$_4$, Ser$_7$, and Lys$_{10}$ create a hydrophilic surface. The carbonyl groups of the macrocycle align, and the amide NH groups of Ser$_7$, D-Thr$_8$, Lys$_{10}$, and Ile$_{11}$ hydrogen bond to the chloride anion. The oxygen atom comprising the ester linkage also faces toward the chloride ion. The amide NH group of Ala$_9$ hydrogen bonds to the hydroxy group of Ser$_7$.

The peptide molecules form hydrogen-bonded antiparallel $\beta$-sheet dimers in the crystal lattice (Figure 3). In each dimer,

Received: November 13, 2023
Revised: March 1, 2024
Accepted: March 7, 2024
Published: March 20, 2024

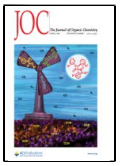





https://doi.org/10.1021/acs.joc.3c02617
J. Org. Chem. 2024, 89, 5104−5108

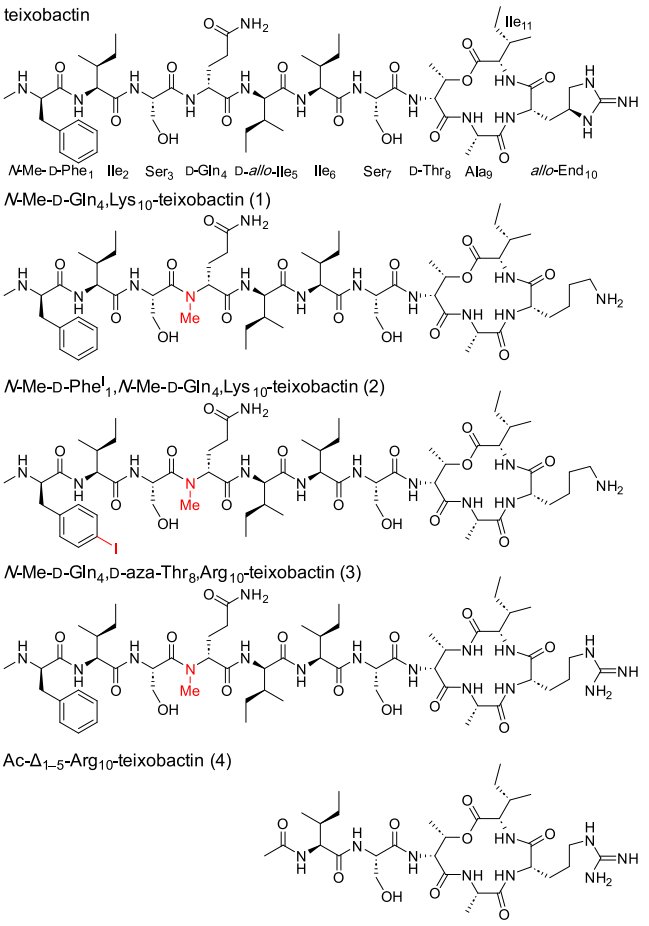


**Figure 1.** Chemical structures of teixobactin, *N*-methylated D-$Gln_4$ analogues of teixobactin, and a truncated teixobactin analogue.

residues 1−3 come together through hydrogen bonding interactions to create the antiparallel $\beta$-sheet structure. The *N*-methyl groups of *N*-Me-D-$Gln_4$ point outward from the hydrogen-bonding interface. The dimer is amphiphilic, with the top surface shown in Figure 3 being hydrophilic and the bottom surface being hydrophobic.

The dimers further assemble end-to-end in the crystal lattice, as illustrated in Figure 4. In this arrangement, the macrocycle of each molecule is in contact with the N-terminus of another molecule in the adjacent dimer, with the carbonyl group of $Ala_9$ hydrogen bonding to the *N*-methylammonium group. Two macrocycles are in proximity at each interface between dimers, with the bound chloride anions being ca. 7 Å apart. The end-to-end assembly of dimers is amphiphilic, and the hydrophobic surfaces pack together in the crystal lattice.

The dimers and other supramolecular interactions of *N*-Me-D-$Gln_4$,$Lys_{10}$-teixobactin (1) observed in the crystal state differ in several ways from those of *N*-methylated teixobactin analogues **2** and **3** (Figure 5). In the antiparallel $\beta$-sheet dimer of teixobactin analogue **1**, residues 1−3 hydrogen bond, with *N*-Me-D-$Phe_1$ pairing with $Ser_3$. Analogue **2** also forms an antiparallel $\beta$-sheet dimer, but there is more overlap of the strands with residues 1−6 forming the dimer interface (PDB 6E00). The dimers further assemble through antiparallel $\beta$-sheet interactions involving residues 3−7 of their outer edges. Analogue **3** forms an antiparallel $\beta$-sheet dimer with residues 3−5 forming the dimer interface (PDB 6PSL). In the dimers formed by analogues **2** and **3**, the N-terminus of one peptide

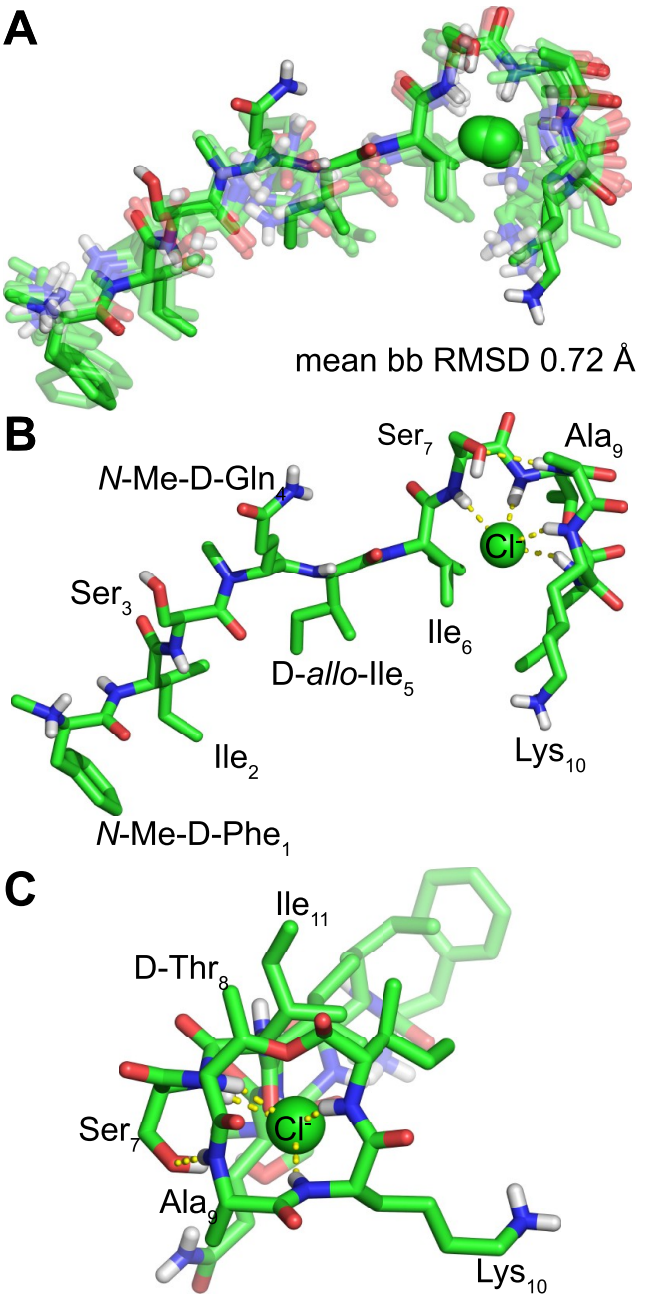


**Figure 2.** X-ray crystallographic structure of teixobactin analogue **1** (PDB 8U78). (A) Overlay of the eight peptide molecules binding chloride anions in the asymmetric unit. (B) Side view and (C) end view of a representative peptide molecule.

molecule helps bind the anion that is grasped by the C-terminal region of the other molecule. In the dimers formed by analogue **1**, however, only the C-terminal region participates in anion binding. The dimers of analogues **1** and **2** further assemble in the lattice to create amphiphilic sheets that pack through hydrophobic interactions. The dimers of analogue **3** further assemble through hydrophobic interactions to create threefold symmetrical rods that extend through the crystal lattice.

Despite these differences, similarities exist across all of the X-ray crystallographic structures that we have determined. The analogues **1**−**3** each come together through antiparallel $\beta$-sheet interactions to create amphiphilic $\beta$-sheet dimers. The


https://doi.org/10.1021/acs.joc.3c02617
J. Org. Chem. 2024, 89, 5104−5108

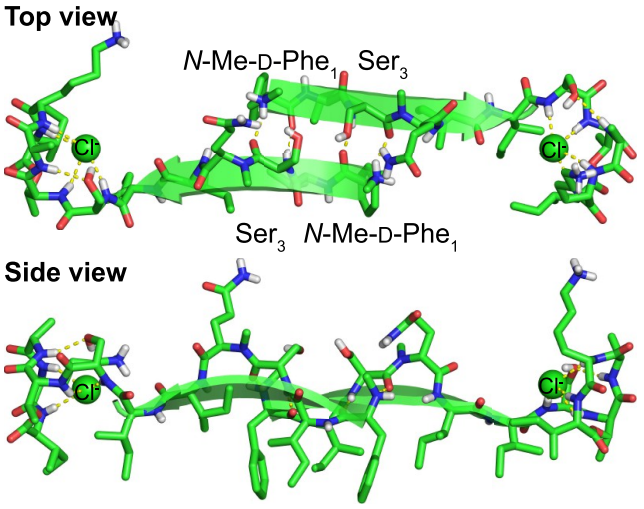


**Figure 3.** Hydrogen-bonded antiparallel $\beta$-sheet dimer in the crystal lattice of teixobactin analogue **1**.

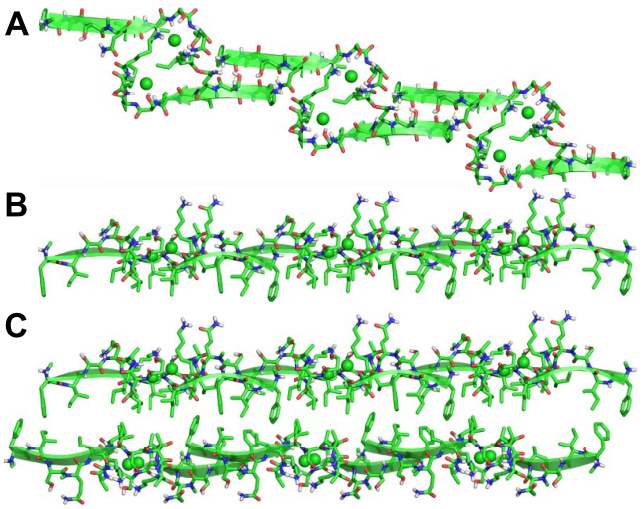


**Figure 4.** End-to-end dimer assemblies and their packing in the crystal lattice. (A) Top view. (B) Side view. (C) Hydrophobic packing in the crystal lattice.

dimerization of these analogues likely reflects the propensity of teixobactin to form dimers and higher-order assemblies that interact with bacterial cell membranes through hydrophobic interactions. Analogues **1**−**3** and truncated analogue **4** (CCDC 1523518) each bind anions in the crystal state, with analogues **1**, **3**, and **4** binding chloride and analogue **2** binding sulfate. The binding of these anions likely reflects the propensity of teixobactin to bind the pyrophosphate groups of lipid II and related cell wall precursors.

Supramolecular assembly is integral to the mechanism of action of teixobactin. *N*-Methylation at D-$Gln_4$ helps prevent uncontrolled aggregation, permits the crystallization of teixobactin analogues, and allows the observation of conformation and supramolecular interactions at atomic resolution. In the crystal state, the teixobactin analogues adopt an amphiphilic conformation and form antiparallel $\beta$-sheet dimers though hydrogen bonding between the N-terminal tails. The macrocycles formed by residues 8−11 bind anions through hydrogen bonding. The hydrophobic surfaces of the dimers further pack through hydrophobic interactions. These observations further support a model in which teixobactin binds to Gram-positive bacteria through interactions of its hydrophobic side chains with the bacterial cell membrane, undergoes supramolecular assembly through $\beta$-sheet interactions, and binds the pyrophosphate groups of lipid II and related cell-wall precursors.

## EXPERIMENTAL SECTION

**General Information.** Methylene chloride ($CH_2Cl_2$) was passed through alumina under argon prior to use. Amine-free *N*,*N*-dimethylformamide (DMF) was purchased from Alfa Aesar. Fmoc-D-*allo*-Ile-OH was purchased from Santa Cruz Biotechnology. Fmoc-*N*-Me-D-Gln(Trt)-OH was purchased from ChemPep. Other protected amino acids were purchased from CHEM-IMPEX. Preparative reversed-phase HPLC was performed on a Rainin Dynamax instrument equipped with an Agilent Zorbax SB-C18 column. Analytical reverse-phase HPLC was performed on an Agilent 1260 Infinity II instrument equipped with a Phenomonex Aeris PEPTIDE 2.6$\mu$ XB-C18 column. HPLC grade acetonitrile (MeCN) and deionized water (18 MΩ) containing 0.1% trifluoroacetic acid (TFA) were used as solvents for both preparative and analytical reverse-phase HPLC. Deionized water (18 MΩ) was obtained from a Barnstead NANOpure Diamond purification system or a ThermoScientific Barnstead GenPure Pro water purification system. Glass solid-phase peptide synthesis vessels with fritted disks and BioRad Polyprep columns were used for the solid-phase peptide synthesis. Teixobactin analogue **1** was prepared and studied as the trifluoroacetate salt.

**Synthesis and Crystallization of *N*-Me-D-$Gln_4$,$Lys_{10}$-teixobactin (1).** We synthesized *N*-Me-D-$Gln_4$,$Lys_{10}$-teixobactin (**1**) as the trifluoroacetate (TFA) salt as described.[7] Crystallization was performed by using standard protein crystallography techniques. Briefly, *N*-Me-D-$Gln_4$,$Lys_{10}$-teixobactin (**1**) was dissolved in 18 MΩ deionized $H_2O$ at a concentration of 20 mg/mL. Suitable crystallization conditions were identified by screening experiments in a 96-well plate format with the aid of using screening kits from Hampton Research (including PEG/Ion, Index, and Crystal Screen kits). Each well was loaded with 100 $\mu$L of a solution from the kits. Hanging drops were set up using a TTP Labtech Mosquito liquid handling instrument, with three 150 nL drops per well with 1:1, 1:2, and 2:1 ratios of well solution and peptide stock solution. Crystals grew in conditions containing chloride with PEG3350 as a precipitant.

To optimize the crystal growth, we tested various conditions that included PEG3350 and $MgCl_2$. In this optimization process, we varied the concentrations of PEG3350 (from 15% to 30%) and $MgCl_2$ (from 0.20 to 0.38 M) across a 4 × 6 matrix within a Hampton VDX 24-well plate. Hanging drops for the optimization experiments were prepared on glass slides by combining 1 or 2 $\mu$L of the *N*-Me-D-$Gln_4$,$Lys_{10}$-teixobactin solution with 1 or 2 $\mu$L of the well solution using ratios of 1:1, 2:1, and 1:2. Crystals were assessed for X-ray diffraction using a Rigaku Micromax-007 HF diffractometer equipped with a Cu anode.

**X-ray Data Collection and Processing.** Data collection was conducted using the BOS/B3 software at the Advanced Light Source (ALS) on beamline 8.2.2. We collected X-ray diffraction at the longest wavelength possible (2.0663 Å, 6000 eV) to allow for the use of chloride K-edge X-ray absorption (2822 eV) for single anomalous diffraction (SAD) phasing. Three data sets were acquired from three different crystals. Two sets of 360 images were acquired per crystal with 1.0° rotation intervals (equivalent to two complete 360° rotations). The data sets were processed using XDS,[8] and the resulting data sets were merged employing BLEND.[9] To determine the structure, we used SAD phasing, implementing the Hybrid Substructure Search (HySS)[10] module from the Phenix suite.[11] The anomalous signals from the chloride ions were used in this process. Initial electron density maps were generated by incorporating the chloride coordinates as starting positions in Autosol.[12] We also collected a higher-resolution data set at 0.9997 Å wavelength to allow the use of the molecular replacement with the structure determined from the 2.0663 Å data. X-ray diffraction data collection and processing information are summarized in Table S1.



https://doi.org/10.1021/acs.joc.3c02617
J. Org. Chem. 2024, 89, 5104−5108

**A** analogue 1

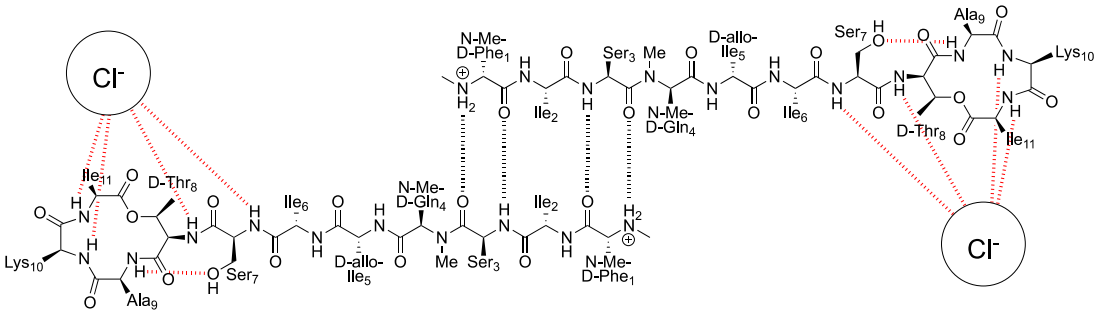


**B** analogue 2

Dimer

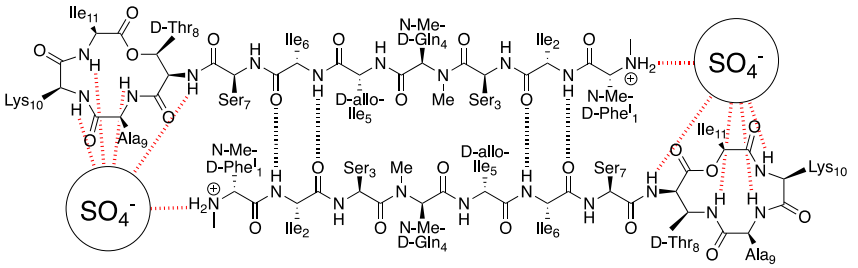


Interface between dimers

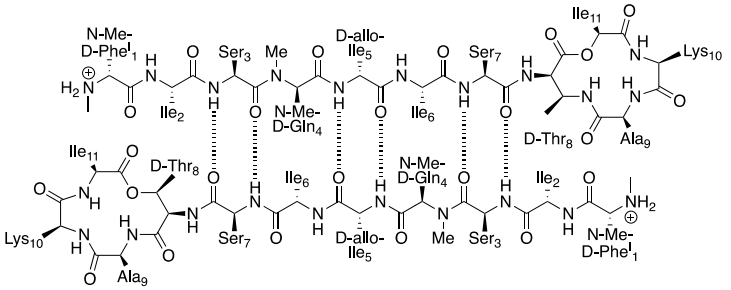


**C** analogue 3

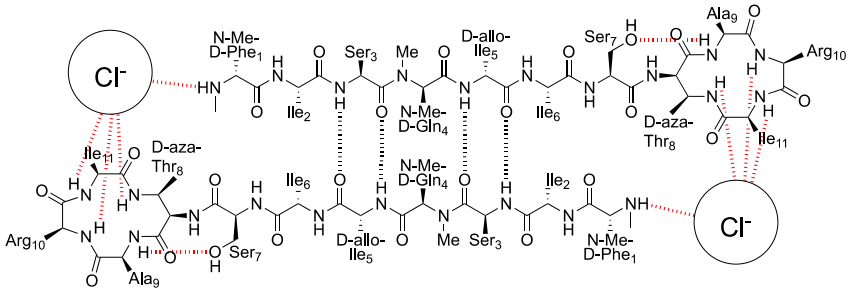


**D** analogue 4

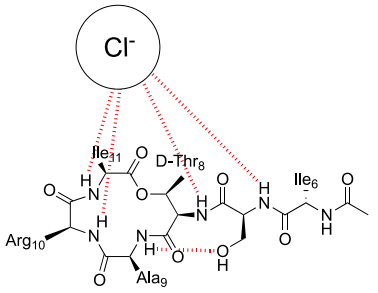


**Figure 5.** Chemical drawings of X-ray crystallographic structures of teixobactin analogues and their antiparallel $\beta$-sheet dimer interactions. (A) Analogue **1**. (B) Analogue **2**. (C) Analogue **3**. (D) Analogue **4**.



https://doi.org/10.1021/acs.joc.3c02617
J. Org. Chem. 2024, 89, 5104−5108

**X-ray Structure Solution and Refinement.** The structure was refined using Phenix.refine,[13] and Coot[14] was used for model building. During refinement, all B-factors were refined isotropically and coordinates for hydrogen atoms were generated geometrically. For the nonproteinogenic amino acids (*N*-Me-D-$Gln_4$, D-$Thr_8$, and D-*allo*-$Ile_5$), bond lengths, angles, and torsion restraints were generated using eLBOW[15] in the Phenix software. The resulting structure was successfully used for molecular replacement with the 0.9997 Å resolution data set, which was refined in a similar fashion. Pentaethylene glycol dimethyl ether was included in the refinement to fill the electron density associated with PEG3350. Final refinement and validation statistics are shown in Table S2 (PDB 8U78).

**HPLC Conditions and MS Results.** Analytical RP-HPLC was performed on a C18 column with an elution gradient of 5−67% $CH_3CN$ + 0.1% TFA over 15 min.

*N-Me-D-Gln$_4$,Lys$_{10}$-teixobactin (1).* MS (ESI) *m*/*z*: $[M + H]^+$ calcd for $C_{59}H_{100}N_{13}O_{15}$ 1230.75, found 1230.5.

## ■ ASSOCIATED CONTENT

### Data Availability Statement

The data underlying this study are available in the published article and its Supporting Information.

### Supporting Information

The Supporting Information is available free of charge at https://pubs.acs.org/doi/10.1021/acs.joc.3c02617.

HPLC and MS characterization data and X-ray crystallographic statistics for *N*-Me-D-$Gln_4$,$Lys_{10}$-teixobactin (**1**) (PDF)

### Accession Codes

Crystallographic coordinates of *N*-Me-D-$Gln_4$,$Lys_{10}$-teixobactin (**1**) were deposited into the Protein Data Bank (PDB) with code 8U78.

## ■ AUTHOR INFORMATION


### Corresponding Author

**James S. Nowick** − *Department of Chemistry and Department of Pharmaceutical Sciences, University of California Irvine, Irvine, California 92697, United States;* orcid.org/0000-0002-2273-1029; Email: jsnowick@uci.edu

### Authors

**Hyunjun Yang** − *Department of Chemistry, University of California Irvine, Irvine, California 92697, United States;* orcid.org/0000-0003-2524-2201

**Adam G. Kreutzer** − *Department of Chemistry, University of California Irvine, Irvine, California 92697, United States;* orcid.org/0000-0002-9724-6298

Complete contact information is available at: https://pubs.acs.org/10.1021/acs.joc.3c02617


### Notes

The authors declare no competing financial interest.

## ■ ACKNOWLEDGMENTS

This work was supported by the National Institutes of Health (Grants AI121548 and AI137258). H.Y. acknowledges Allergan for fellowship support. We thank the Berkeley Center for Structural Biology (BCSB) of the Advanced Light Source (ALS) for synchrotron data collection. The BCSB is supported in part by the Howard Hughes Medical Institute. The ALS is supported by DOE Office of Science User Facility under contract no. DE-AC02-05CH11231. Previous versions of this manuscript are available in bioRxiv at https://doi.org/10.1101/2023.10.30.564786.

## ■ REFERENCES


(1) Ling, L. L.; Schneider, T.; Peoples, A. J.; Spoering, A. L.; Engels, I.; Conlon, B. P.; Mueller, A.; Schäberle, T. F.; Hughes, D. E.; Epstein, S.; Jones, M.; Lazarides, L.; Steadman, V. A.; Cohen, D. R.; Felix, C. R.; Fetterman, K. A.; Millett, W. P.; Nitti, A. G.; Zullo, A. M.; Chen, C.; Lewis, K. A new antibiotic kills pathogens without detectable resistance. *Nature* **2015**, *517*, 455−459.

(2) Shukla, R.; Medeiros-Silva, J.; Parmar, A.; Vermeulen, B. J. A.; Das, S.; Paioni, A. L.; Jekhmane, S.; Lorent, J.; Bonvin, A. M. J. J.; Baldus, M.; Lelli, M.; Veldhuizen, E. J. A.; Breukink, E.; Singh, I.; Weingarth, M. Mode of action of teixobactins in cellular membranes. *Nat. Commun.* **2020**, *11*, 2848.

(3) Shukla, R.; Lavore, F.; Maity, S.; Derks, M. G. N.; Jones, C. R.; Vermeulen, B. J. A.; Melcrová, A.; Morris, M. A.; Becker, L. M.; Wang, X.; Kumar, R.; Medeiros-Silva, J.; van Beekveld, R. A. M.; Bonvin, A. M. J. J.; Lorent, J. H.; Lelli, M.; Nowick, J. S.; MacGillavry, H. D.; Peoples, A. J.; Spoering, A. L.; Ling, L. L.; Hughes, D. E.; Roos, W. H.; Breukink, E.; Lewis, K.; Weingarth, M. Teixobactin kills bacteria by a two-pronged attack on the cell envelope. *Nature* **2022**, *608*, 390−396.

(4) Yang, H.; Wierzbicki, M.; Du Bois, D. R.; Nowick, J. S. X-ray Crystallographic Structure of a Teixobactin Derivative Reveals Amyloid-like Assembly. *J. Am. Chem. Soc.* **2018**, *140*, 14028−14032.

(5) Yang, H.; Pishenko, A. V.; Li, X.; Nowick, J. S. Design, Synthesis, and Study of Lactam and Ring-Expanded Analogues of Teixobactin. *J. Org. Chem.* **2020**, *85*, 1331−1339.

(6) Yang, H.; Du Bois, D. R.; Ziller, J. W.; Nowick, J. S. X-ray crystallographic structure of a teixobactin analogue reveals key interactions of the teixobactin pharmacophore. *Chem. Commun.* **2017**, *53*, 2772−2775.

(7) Yang, H.; Chen, K. H.; Nowick, J. S. Elucidation of the Teixobactin Pharmacophore. *ACS Chem. Biol.* **2016**, *11*, 1823−1826.

(8) Kabsch, W. XDS. *Acta Crystallogr., Sect. D: Biol. Crystallogr.* **2010**, *66*, 125−132.

(9) Foadi, J.; Aller, P.; Alguel, Y.; Cameron, A.; Axford, D.; Owen, R. L.; Armour, W.; Waterman, D. G.; Iwata, S.; Evans, G. Clustering procedures for the optimal selection of data sets from multiple crystals in macromolecular crystallography. *Acta Crystallogr., Sect. D: Biol. Crystallogr.* **2013**, *69*, 1617−1632.

(10) Grosse-Kunstleve, R. W.; Adams, P. D. Substructure search procedures for macromolecular structures. *Acta Crystallogr., Sect. D: Biol. Crystallogr.* **2003**, *59*, 1966−1973.

(11) Adams, P. D.; Afonine, P. V.; Bunkoczi, G.; Chen, V. B.; Davis, I. W.; Echols, N.; Headd, J. J.; Hung, L. W.; Kapral, G. J.; Grosse-Kunstleve, R. W.; McCoy, A. J.; Moriarty, N. W.; Oeffner, R.; Read, R. J.; Richardson, D. C.; Richardson, J. S.; Terwilliger, T. C.; Zwart, P. H. PHENIX: a comprehensive Python-based system for macromolecular structure solution. *Acta Crystallogr., Sect. D: Biol. Crystallogr.* **2010**, *66*, 213−221.

(12) Terwilliger, T. C.; Adams, P. D.; Read, R. J.; McCoy, A. J.; Moriarty, N. W.; Grosse-Kunstleve, R. W.; Afonine, P. V.; Zwart, P. H.; Hung, L. W. Decision-making in structure solution using Bayesian estimates of map quality: the PHENIX AutoSol wizard. *Acta Crystallogr., Sect. D: Biol. Crystallogr.* **2009**, *65*, 582−601.

(13) Afonine, P. V.; Grosse-Kunstleve, R. W.; Echols, N.; Headd, J. J.; Moriarty, N. W.; Mustyakimov, M.; Terwilliger, T. C.; Urzhumtsev, A.; Zwart, P. H.; Adams, P. Towards automated crystallographic structure refinement with phenix.refine. *Acta Crystallogr., Sect. D: Biol. Crystallogr.* **2012**, *68*, 352−367.

(14) Emsley, P.; Lohkamp, B.; Scott, W. G.; Cowtan, K. Features and development of Coot. *Acta Crystallogr., Sect. D: Biol. Crystallogr.* **2010**, *66*, 486−501.

(15) Moriarty, N. W.; Grosse-Kunstleve, R. W.; Adams, P. D. electronic Ligand Builder and Optimization Workbench (eLBOW): a tool for ligand coordinate and restraint generation. *Acta Crystallogr., Sect. D: Biol. Crystallogr.* **2009**, *65*, 1074−1080.